Molecular & Biochemical Parasitology 258 (2024) 111619

Contents lists available at ScienceDirect

Molecular & Biochemical Parasitology

journal homepage: www.elsevier.com/locate/molbiopara

Formation of functional E3 ligase complexes with UBC2 and UEV1 of *Leishmania mexicana*

Rebecca J. Burge [a], Katie H. Jameson [b], Vincent Geoghegan [a], Adam A. Dowle [c], Jeremy C. Mottram [a,*], Anthony J. Wilkinson [b,*]

[a] York Biomedical Research Institute, Department of Biology, University of York, York YO10 5DD, UK
[b] York Structural Biology Laboratory and York Biomedical Research Institute, Department of Chemistry, University of York, York YO10 5DD, UK
[c] Bioscience Technology Facility, Department of Biology, University of York, York YO10 5DD, UK

ARTICLE INFO

Keywords:
Ubiquitin
Leishmania
Ubiquitin ligase
Ubiquitin-conjugating enzyme (E2 enzyme)
Interactome
Proteomics

ABSTRACT

In eukaryotic cells, molecular fate and cellular responses are shaped by multicomponent enzyme systems which reversibly attach ubiquitin and ubiquitin-like modifiers to target proteins. The extent of the ubiquitin proteasome system in *Leishmania mexicana* and its importance for parasite survival has recently been established through deletion mutagenesis and life-cycle phenotyping studies. The ubiquitin conjugating E2 enzyme UBC2, and the E2 enzyme variant UEV1, with which it forms a stable complex *in vitro*, were shown to be essential for the differentiation of promastigote parasites to the infectious amastigote form. To investigate further, we used immunoprecipitation of Myc-UBC2 or Myc-UEV1 to identify interacting proteins in *L. mexicana* promastigotes. The interactome of UBC2 comprises multiple ubiquitin-proteasome components including UEV1 and four RING E3 ligases, as well as potential substrates predicted to have roles in carbohydrate metabolism and intracellular trafficking. The smaller UEV1 interactome comprises six proteins, including UBC2 and shared components of the UBC2 interactome consistent with the presence of intracellular UBC2-UEV1 complexes. Recombinant RING1, RING2 and RING4 E3 ligases were shown to support ubiquitin transfer reactions involving the E1, UBA1a, and UBC2 to available substrate proteins or to unanchored ubiquitin chains. These studies define additional components of a UBC2-dependent ubiquitination pathway shown previously to be essential for promastigote to amastigote differentiation.

1. Introduction

The leishmaniases are a spectrum of diseases caused by more than twenty *Leishmania* parasite species with disease manifesting as cutaneous, mucocutaneous and visceral forms [1,2]. It is endemic in more than 80 countries and, despite its association with high morbidity and mortality, leishmaniasis remains a neglected tropical disease (www.who.int/health-topics/leishmaniasis). In the absence of a licensed vaccine, measures to counter leishmaniasis rely on chemotherapy but drugs in current use suffer from toxic side effects, difficulties in administration and extended treatment times – moreover, resistance is emerging. New anti-leishmanial drugs are a recognised priority [3], and one of the most promising compounds to enter clinical trials is LXE408, a proteasome inhibitor [4].

Leishmania are transmitted through the bite of female phlebotomine sandflies when they take a blood meal. The promastigote form of the parasite, which is injected into the skin, is taken up by macrophages where it becomes enclosed in a parasitophorous vesicle (PV). In the PV, the parasite undergoes differentiation to the human infectious amastigote form. Amastigotes multiply before bursting from the cell to initiate new cycles of infection, either of cells in the immediate neighbourhood in the case of cutaneous leishmaniasis, or after dissemination to distant tissues such as the liver, spleen and bone marrow in the case of visceral leishmaniasis. The cycle of infection continues when amastigote parasites are taken up by a feeding sandfly. In the insect gut, temperature and pH cues trigger the pathway of differentiation to the promastigote form. Parasite differentiation is characterised by substantial changes in cell morphology accompanied by changes in the composition of the parasite proteome orchestrated by post-translational modification systems [5,6]. The interest here is in the role of ubiquitination in cell differentiation.

Ubiquitin is a small protein with a β-grasp fold and a sequence that is highly conserved across species [7]. Its attachment to target proteins

* Corresponding authors.
E-mail addresses: jeremy.mottram@york.ac.uk (J.C. Mottram), tony.wilkinson@york.ac.uk (A.J. Wilkinson).

https://doi.org/10.1016/j.molbiopara.2024.111619
Received 8 January 2024; Received in revised form 14 March 2024; Accepted 26 March 2024
Available online 29 March 2024

alters molecular function and cell fate. Ubiquitination is the result of the sequential action of ubiquitin-activating (E1), ubiquitin-conjugating (E2) and ubiquitin-ligating (E3) components [8]. Ubiquitin can be attached in multiple copies and in different linkages to target proteins giving rise to enormous complexity in what has been termed the Ubiquitin Code [9]. Lys48-linked polyubiquitination for example, is associated with proteasomal protein degradation while Lys-63-linked ubiquitination plays a role in protein recruitment to sites of DNA damage. Ubiquitination is reversible with ubiquitin returned to the cellular pool by the activities of deubiquitinases [10]. Besides ubiquitin, an array of structurally similar, but sequence-divergent, ubiquitin-like modifiers (Ubls) exist, each with a complement of cognate E1, E2, and E3 components and Ubl-specific proteases [11].

In trypanosomatids, post-translational modification of target proteins by ubiquitin and Ubls regulates the cell cycle, endocytosis, protein trafficking and degradation, autophagy as well as infection and stress responses [6,12]. In *Leishmania mexicana,* 2 ubiquitin-activating (E1), 13 ubiquitin-conjugating (E2) and 79 ubiquitin-ligating (E3) enzymes have been identified together with up to 30 deubiquitinases (DUBs) [13–15]. The roles of a set of 58 of these ubiquitination components were investigated by using CRISPR-Cas9 mutagenesis to generate E1, E2, or DUB gene deletion parasites. Each was distinguishable by a unique bar code allowing for life-cycle phenotyping experiments. Null mutants of the E1, UBA1a, and the E2s, UBC3, UBC7, UBC12 and UBC13 as well as four DUBs were not obtained, implying essential promastigote roles for these factors [13,14]. To explore the importance of ubiquitination in parasite development, the set of viable null mutant promastigote parasites was pooled and grown to stationary phase before differentiation was induced and the survival of the parasites (i) as axenic amastigotes, (ii) as intra-macrophage amastigotes, and (iii) in mouse footpads was determined [13,14]. Among the ubiquitination components, the Δ*ubc2* and Δ*uev1* mutants exhibited the most severe loss-of-fitness during differentiation [13]. Interestingly, knockdown of the UBC2 orthologue in *T. brucei* using RNAi leads to a severe reduction in viability of this species [16]. UBC2 is an E2 ubiquitin conjugating enzyme and UEV1 is a ubiquitin E2 variant lacking key resides required for activity including the conserved cysteine which participates in the transthiolation reactions. The two proteins form a stable complex whose crystal structure has been determined revealing an interface that is conserved in human and yeast orthologues [13,17–19]. Ubiquitination assays showed that in the presence of *Leishmania* UBA1a and the human E3s RNF8 or BIRC2, UBC2 promoted the formation of polyubiquitin chains on proteins present in the assay. The inclusion of UEV1 restricted the products to K63-linked ubiquitin dimers [13].

The striking effects of *UBC2* and *UEV1* deletion on parasite differentiation to the human infectious form prompted us to explore the roles of these two ubiquitination factors further. Here we have employed a cross-linking proteomics strategy to define the UBC2 and UEV1 interactomes in promastigote parasites. This approach defined a set of potential substrates and E3 ligase partners of UBC2.

2. Results

2.1. Identification of the UBC2 and UEV1 interactomes

To identify RING E3 ligases, other ubiquitin system components and other proteins that interact with UBC2 and UEV1, we used a cross-linking affinity purification proteomics approach. Individual cell lines were generated in which UBC2 or UEV1 were N-terminally tagged with 3xMyc, using CRISPR-Cas9 gene editing [20,21]. MPK3, a protein kinase that is not essential in amastigotes [5], was also tagged as an experimental control, on the assumption that its interacting partners differ from those of UBC2 and UEV1. The presence of 3xMyc on the tagged proteins was validated by Western blotting (Supplementary Figure 1), and an amastigote viability assay showed that the Myc-UBC2 and Myc-UEV1 lines had similar viabilities to the Cas9 T7 parental line during promastigote to amastigote differentiation (Supplementary Figure 2). Since UBC2 and UEV1 are essential in amastigotes [13], this suggested that the N-terminal 3xMyc tag did not affect UBC2 or UEV1 function.

To increase the likelihood of detecting low affinity interactions with RING E3 ligases [22], parasites were treated with dithiobis(succinimidylpropionate), a membrane permeable primary amine-reactive chemical cross-linker, prior to cell lysis and immunocapture on anti-c-Myc antibody coated beads. Following extensive washing, the captured proteins and protein complexes were eluted from beads with an acidic glycine buffer. The immunoprecipitates were further purified by methanol/chloroform precipitation followed by re-solubilisation in the presence of a mass spectrometry compatible surfactant. Proteins were digested with trypsin and LysC proteases and the resulting peptides analysed by liquid chromatography-mass spectrometry. SAINTq [22,23] was used to identify proteins exhibiting significant enrichment, with a false discovery rate of less than 5%, in the Myc-UBC2 or Myc-UEV1 samples *versus* the Myc-MPK3 samples. These data are shown in Tables 1 and 2 and summarized in Fig. 1.

For UBC2, significant interactors included seven ubiquitin system components: UEV1, ubiquitin, UBC13 and four potential RING-type E3 ligases (LmxM.24.1380, LmxM.24.1390, LmxM.18.1150 and LmxM.24.0080). Among these E3 ligase genes, LmxM.24.1380 and LmxM.24.1390 are found in a tandem array and share 82% amino acid sequence identity, with the principal difference being a 57-residue insertion in LmxM.24.1380 in the central segment of the protein (Supplementary Figure 3). The peptides in the dataset could not distinguish these two E3 ligases. The RING E3 ligases LmxM.24.1380, LmxM.18.1150, LmxM.24.0080 and LmxM.24.1390 were named RINGs 1–4, respectively.

Leishmania have 4 ubiquitin genes. Three encode C-terminal fusions of ubiquitin to the L40 component of the 60 S ribosomal subunit (LmxM.09.0891, LmxM.30.2030 and LmxM.30.1900). One encodes a polyubiquitin, which is poorly annotated in the *L. mexicana* genome (LmxM.36.3530), but is orthologous to the polyubiquitin of *L. major* (LmjF.36.3530). Regardless, these gene products are indistinguishable in the proteomics dataset as the identified peptides map to the N-terminal ubiquitin elements, which have identical sequences.

Significant ubiquitin system interactors of UEV1 include UBC2 and UBC13. Other UBC2 and UEV1 interactors within the dataset are likely

Table 1
Proteins enriched in UBC2 versus MPK3 promastigote immunoprecipitations, as analysed by protein-level analysis in SAINTq. A 5% false discovery rate was used as the cut-off.

Accession	Fold change	Name
LmxM.13.1580	932.7	UEV1
LmxM.24.0080	294.5	RING-type E3 ligase 3
LmxM.30.1395	276.4	LSD1-like protein
LmxM.34.1300	16.0	UBC13
LmxM.08.29.2160	59.2	rab-GDP dissociation inhibitor
LmxM.26.2490	73.4	hypothetical protein
LmxM.24.1380	20.1	RING-type E3 ligase 1
LmxM.24.1390	20.1	RING-type E3 ligase 4
LmxM.23.0430	42.1	aldose 1-epimerase-like protein
LmxM.09.0891	63.7	ubiquitin-fusion protein 1
LmxM.30.1900	63.7	ubiquitin-fusion protein 2
LmxM.30.2030	63.7	ubiquitin-fusion protein 3
LmxM.36.3530	63.7	polyubiquitin
LmxM.18.1150	47.8	RING-type E3 ligase 2
LmxM.10.0910	6.9	Rab11 GTPase
LmxM.05.0030	4.9	small GTP-binding protein
LmxM.34.2090	5.3	kinesin
LmxM.23.0200	5.0	endoribonuclease L-PSP (pb5)
LmxM.24.0761	3.4	malic enzyme
LmxM.30.2020	1.8	succinyl-diaminopimelate desuccinylase-like protein
LmxM.30.2560	4.2	hypothetical protein

Table 2
Proteins enriched in UEV1 versus MPK3 promastigote immunoprecipitations, as analysed by protein-level analysis in SAINTq. A 5% false discovery rate was used as the cut-off.

Accession	Fold change	Name
LmxM.04.0680	215.0	UBC2
LmxM.08_29.2160	41.1	rab-GDP dissociation inhibitor
LmxM.34.1300	9.7	UBC13
LmxM.28.0980	25.3	hypothetical protein (LmxM.28.0980)
LmxM.10.0290	7.1	isocitrate dehydrogenase
LmxM.26.2490	32.7	hypothetical protein (LmxM.26.2490)

substrates and are involved in key cellular processes associated with intracellular transport, carbohydrate metabolism and gene expression (Fig. 1).

2.2. The UBC2 interacting RING E3 ligases

The AlphaFold predicted structures of the RING E3 ligases identified in the UBC2 interactome were obtained from https://tritrypdb.org/tritrypdb/. The higher confidence regions of these structures (pLDDT > 70) predicted to form discrete domains are shown in Fig. 2. RING1 (LmxM.24.1380) is a 44 kDa protein whose 395 residues are predicted by AlphaFold [24] to form a zinc-binding domain upstream of a 150 residue low complexity region followed by an EF-hand domain pair (Fig. 2**A**). The clustering of cysteine and histidine residues in the model suggests three putative zinc binding sites, two with the characteristic C3HC4 cross brace RING finger coordination and a third CCHC-type zinc finger. The double EF-hand domain has four probable calcium binding sites matching the consensus Dx(D/N)x(S/D)Gx(L/I)(E/S)xxE(V/F). The 37 kDa RING4 shares the zinc binding and the calcium binding domains but has a much shorter low complexity region connecting the two (Fig. 2 and Supplementary Figure 3).

RING2 (LmxM.18.1150) is a 39 kDa protein whose 360 residues are predicted by AlphaFold to form a central immunoglobulin (Ig)-like domain and a C-terminal C3HC4 cross brace RING finger domain. The N-terminal 100 or so residues lack predicted tertiary structure (Fig. 2**B**). In contrast, AlphaFold produces a high confidence structure prediction that spans almost all of the RING3 (LmxM.24.0080) protein chain [24]. Its 55 kDa polypeptide consists of an amino terminal six-bladed β-propeller Kelch domain and a C-terminal domain harbouring six putative zinc-binding sites (Fig. 2**C**).

2.3. Expression and purification of recombinant RING E3s

To determine whether RINGs 1–4 are functional ubiquitination partners of UBC2 and/or UBC2-UEV1, we expressed and purified recombinant proteins from *E. coli*. A variety of expression strategies were followed leading to successful production of soluble RINGs1, 2 and 4 as HRV-3C cleavable GST fusion proteins. Recombinant RING3 and a truncated derivative encompassing residues 236–478 proved to be insoluble in the expression systems explored. RING1, RING2 and RING4 were purified by immobilisation on a glutathione sepharose affinity chromatography column with on-column digestion with HRV-3 C protease used to elute the recombinant RING E3 ligases. The column eluates were subsequently pooled and fractionated on a sepharose S75 gel filtration column (Supplementary Figure 4). The yields per litre of culture for RING2 and RING4 were in the low milligram range while that for RING1 was much lower (~10 μg l^{-1}).

2.4. Ubiquitin transfer by RING E3s

We next explored whether the RING E3s could support ubiquitin transfer reactions in assays involving the E1 ubiquitin activating enzyme, UBA1a, the E2 ubiquitin conjugating enzyme UBC2 and/or the E2 ubiquitin enzyme variant, UEV1. In these assays, the reaction products where resolved by SDS-PAGE, Western blotting and probing with antibodies directed against ubiquitin conjugates [25]. In the presence of Ub, UBA1a promotes the covalent attachment of ubiquitin to UBC2 [13]. The ATP dependence of this reaction is shown in Supplementary Figure 5. In the further presence of UEV1, the UBC2-Ub complex reacts with a second molecule of Ub to form K63-linked diubiquitin [13]. This K63-linked diubiquitin formation also occurs in an assay with the orthologous E2 components, Ubc13 and Mms2 in yeast [26].

Incubation of RING1, RING2 and RING4 with UBA1a, ubiquitin and ATP in the presence of UBC2 led to the appearance of multiple ubiquitin conjugates with mobilities intermediate between those of diubiquitin and the UBA1a-ubiquitin complex (Fig. 3**A**). Qualitatively similar observations were made in earlier assays of UBC2 supported ubiquitination in the presence of the human E3 ligases BIRC2 and RNF8 [13]. The appearance of these conjugates is dependent on the presence of UBC2 and the absence of UEV1. If UEV1 is present, the ubiquitin is diverted into ubiquitin dimers including K63-linked dimers as evidenced by probing of the Western blots with anti-K63 linked diubiquitin antibody (Fig. 3**B**). Curiously, a prominent species with a mobility of around 55 kDa reacts with the anti-K63 antibodies in the RING2 reactions independently of the presence of UBC2 and UEV1.

In summary, the three purified RING E3 ligases are able to cooperate with UBC2 to give rise to ubiquitin conjugates (Fig. 3**C**). The profile of the products of the RING1 and RING4 reactions are similar consistent with the structural similarity of the two enzymes and distinct from those produced by RING2. The nature of the ubiquitin linkages is not known, nor are the identities of Ub-linked species. Since the cognate substrates are not present these would have to be free ubiquitin chains or autoubiquitination products of the E1, E2 or E3 components. Further work is needed to characterise these reactions products.

2.5. Comparison of AlphaFold predicted E3 structures to known E3 structures

To identify the most closely related structures in the Protein Data Bank to the AlphaFold predicted structures of the RING E3 ligases identified here, we used the programme PDBeFold. The search with the RING domain of RING2 (residues 299–350) identified, as expected, numerous RING domains with BIRC4 and MDM2 among the highest scoring hits.

For the closely similar RINGs 1 and 4, we searched with the RING Zinc finger (RING-ZnF) fragment (residues 1–93) as the query. The most closely similar matches were the human E3s TRAF6 (3hcu) and RNF125 (5dka). Both proteins possess C2HC zinc-finger domains C-terminal to their RING domains. TRAF6 mediates Lys63-linked polyubiquitination of itself and other signalling proteins as part of NF-κB activation. In doing so, it uses the E2 Ubc13 and Uev1A which is significant in terms of the results presented here. In the crystal structure of a TRAF6 RING-ZnF: Ubc13 complex [27], the zinc finger forms no direct contacts with Ubc13. Instead it stabilises the conformation of residues preceding the RING domain which do form stabilising contacts with the E2. RNF125 is involved in the regulation of multiple processes including T-cell activation, HIV transcription and p53 degradation. In RNF125, the zinc finger domain packs more closely with the RING domain and stabilises its structure. Moreover, NMR data suggest both the RING and ZnF elements participate in interactions with the cognate E2 protein [28].

For RING3, we searched the PDB for structures with the closest similarity to residues 269–501 of the AlphaFold model. The closest match (rmsΔ = 2.9 Å for 116 matching residues) is the structure of the C-terminal RING-Cys-Relay (RCR) domain of the 0.5 MDa E3 ligase MYCBP2 (6t7f) [29]. This E3 ligase, with a role in neurodevelopment, undergoes a transthiolation reaction with its cognate E2-Ub substrate with the Ub becoming successively attached to two Cys residues in its tandem cysteine (TC) domain which is C-terminal to the RING domain [30]. The Ub is subsequently relayed to a threonine residue on an acceptor substrate in a transesterifaction reaction [30].

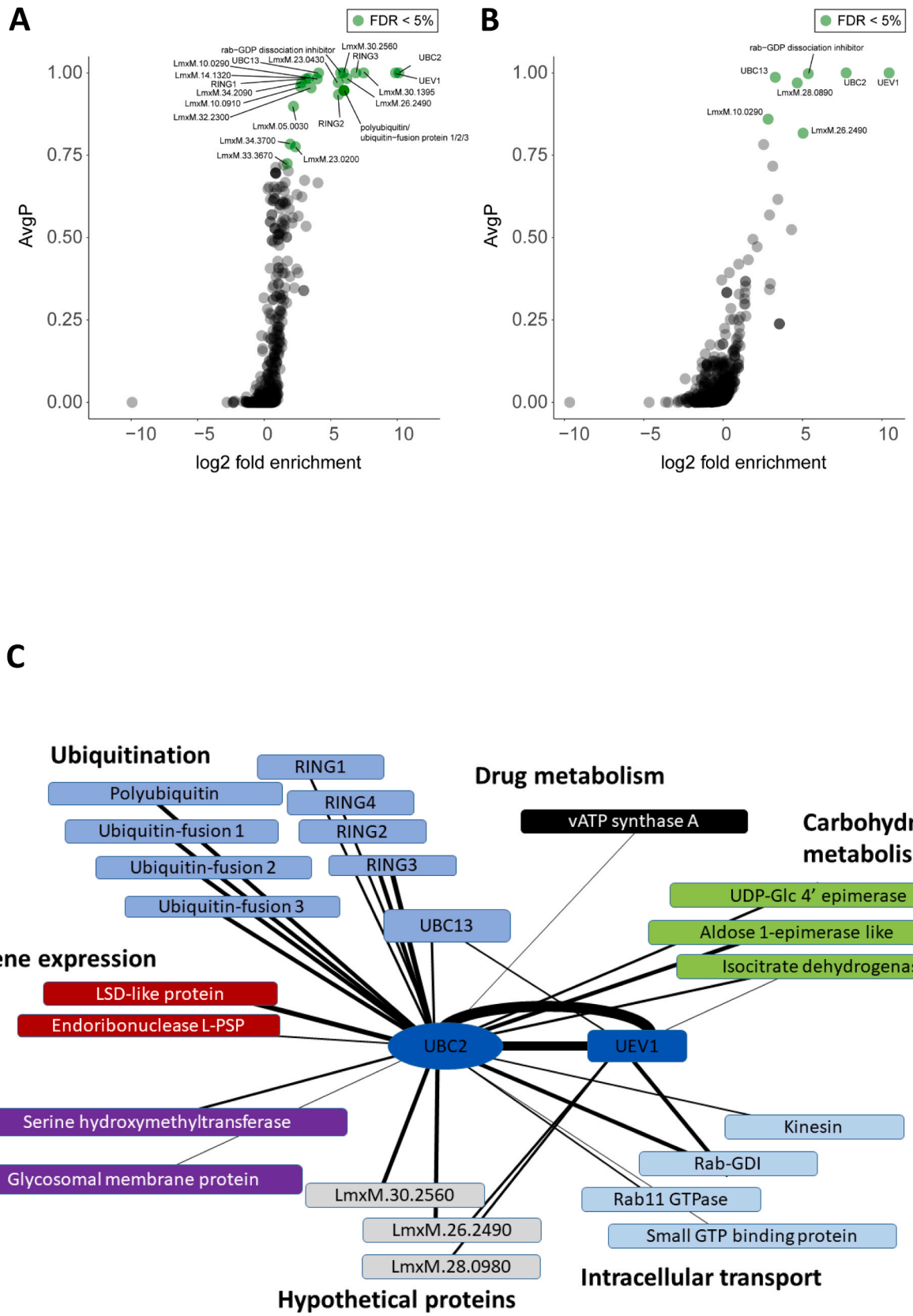

Fig. 1. *UBC2 and UEV1 interactomes in L. mexicana promastigotes.* Putative interacting partners of **A** UBC2 and **B** UEV1 as determined by protein-level SAINTq analysis (data in Table 1 and Table 2). Green points indicate proteins that were significantly enriched in the UBC2 or UEV1 versus the MPK3 immunoprecipitations (< 5% false discovery rate). AvgP, is the average probability of true interaction. **C.** The UBC2 and UEV1 interactome. The thickness of lines is proportional to the log2 fold change between the protein abundances in UBC2 or UEV1 versus MPK3 immunoprecipitation samples. Key cellular processes (identified using GO term analysis and literature searching) with which proteins or putative proteins are associated are indicated next to the relevant nodes.

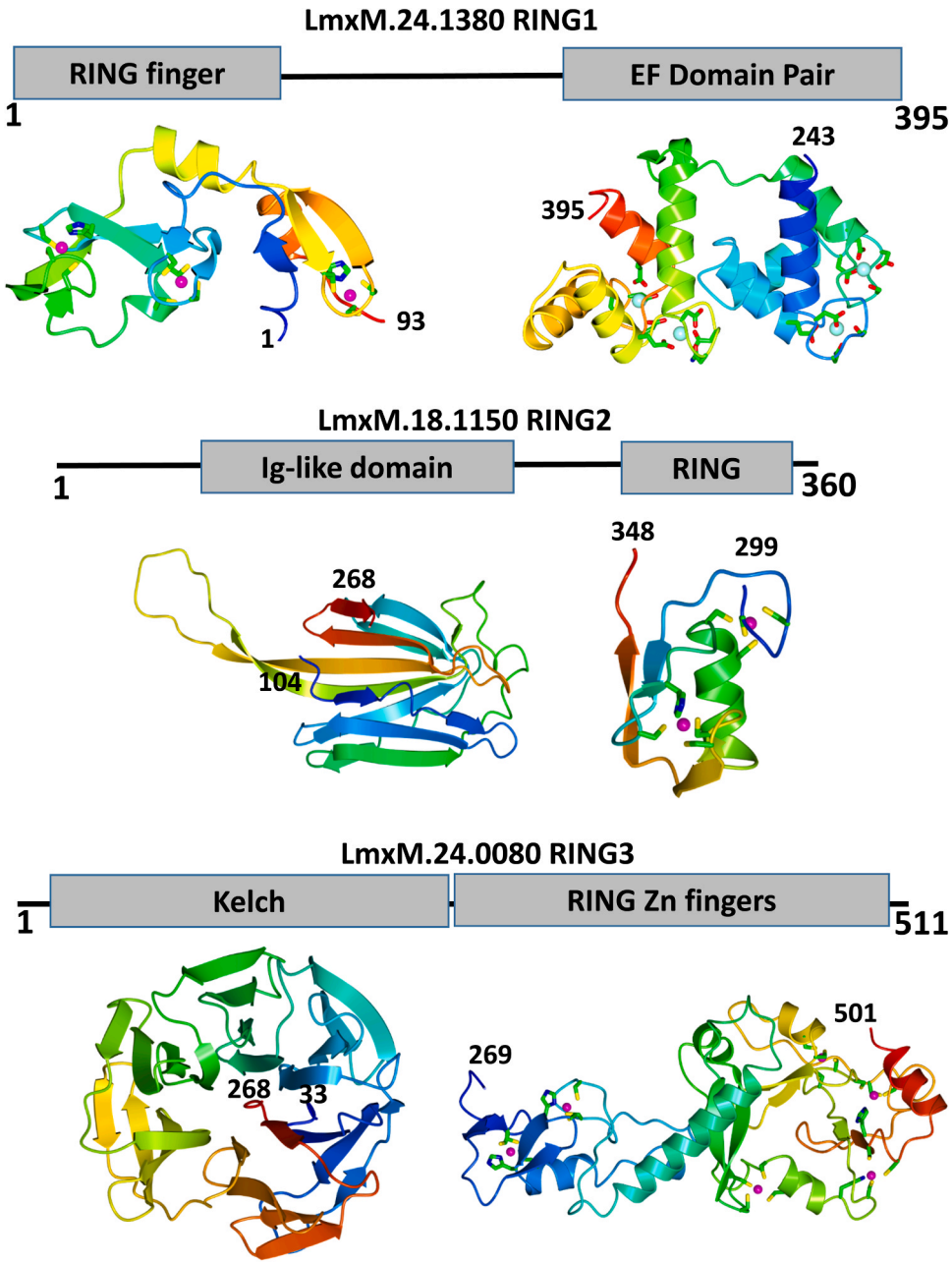

Fig. 2. The domain organisation and AlphaFold-predicted domain structures of the UBC-interacting RING E3s. The domain structures for RING1 (**A**), RING2 (**B**) and RING3 (**C**) are derived from the high confidence regions of AlphaFold (24) coordinate sets AF-E9AWY1-F1, AF-E9ARQ2-F1 and AF-E9AWJ8-F1 respectively. The predicted structure of RING4 is not shown here as its high confidence regions are identical to those of RING1, the difference being that the central disordered region of RING4 is much shorter as is evident in Supplementary Figure 3. Calcium and zinc ions were manually introduced into the EF-hand and RING/Zinc finger domains respectively in the programme Coot [43]. Metal coordinating side chains are shown in cylinder format coloured by atom (carbon, green; oxygen, red; nitrogen, blue and sulphur, yellow) with the calcium and zinc ions respectively shown as aquamarine and magenta spheres. The images were produced with CC4mg [44].

The structural similarity with *L. mexicana* RING3 extends across the whole of the RCR region, though the juxtaposition of the RING domain with the putative TC domain is altered (Fig. 4**A**). This structural similarity is matched by sequence similarity with conservation of the cysteine and histidine residues involved in coordinating the two zinc atoms in the RING domain and the four zinc atoms in the TC domain (Fig. 4**B**). The exception is a swapping of the order of the Cys and His residues coordinating Zn4. Intriguingly, Cys390 of RING3 aligns exactly with Cys4520, the first of the two acceptor cysteines of MYCBP2 suggesting that this residue in RING3 participates as an acceptor in Ub transfer [29]. RING3 lacks a match for the second acceptor cysteine (Cys4572) with the corresponding residue being Ser438. There is interestingly a cysteine residue (Cys479) in RING3 that is not conserved in MYCBP2, which is spatially close to the Cys4572 in three dimensions and represents a candidate downstream Ub acceptor (Fig. 4).

To explore whether the domain structure of the *L. mexicana* RINGs 1–4 is shared by any of the human E3 ligases, we carried out BLAST searches. Outside of the RING/Zinc binding domains discussed above, we found no significant additional sequence conservation with human E3s. Thus, either the domain combinations in the *Leishmania* RING E3s are distinct, or their sequences have diverged from those found in human E3s beyond the point where structural conservation is discernible.

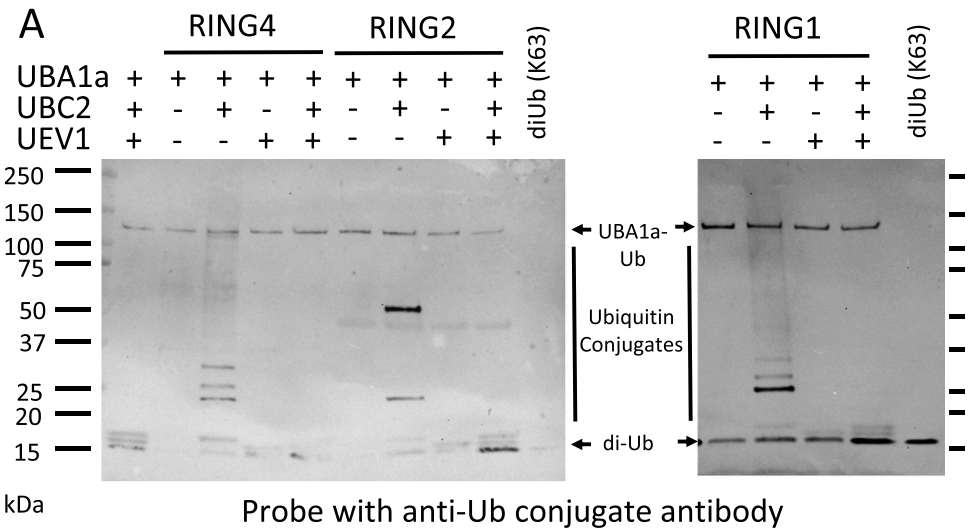

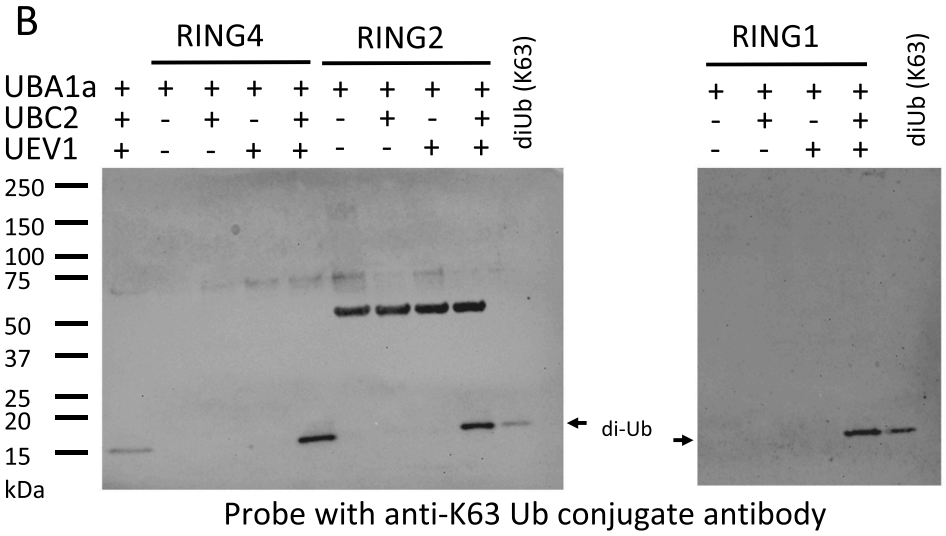

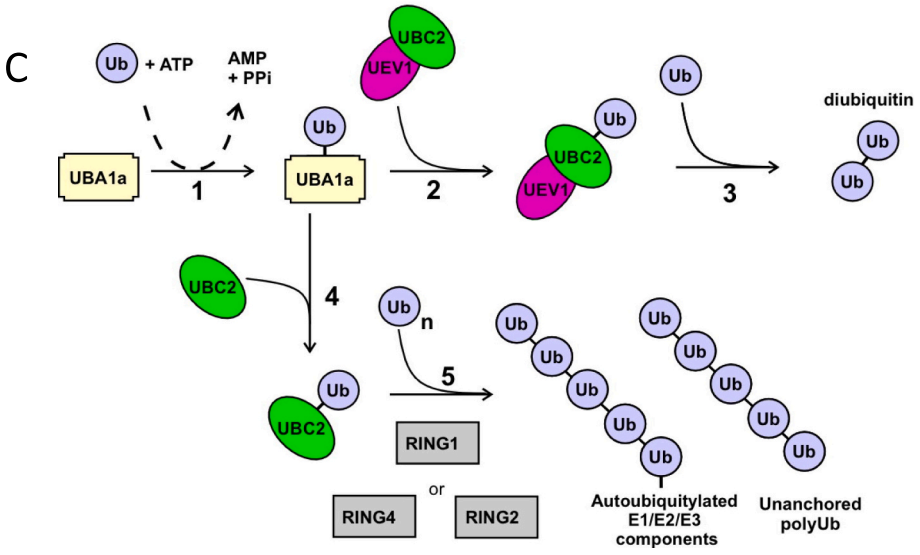

(caption on next page)

Fig. 3. *Ubiquitination assays of RING1, RING2 and RING4.* The ubiquitin ligase UBA1a, ubiquitin, the indicated RING E3 ligase, and ATP were incubated in the presence or absence of UBC2 and/or UEV1 and the products resolved by SDS polyacrylamide gel electrophoresis. The proteins were electroblotted onto membranes and the ubiquitinated protein products were visualised by chemiluminescence following probing of the membrane with antibody FK2, which detects all ubiquitin conjugates (**A**) or against a Ub-K63 antibody which specifically detects K63-linked ubiquitin conjugates (**B**). **C.** Schematic of the ubiquitination assays for the RING E3 ligases in the absence of cognate substrates. In the presence of ATP, UBA1a activates ubiquitin (Ub) forming a UBA1a-Ub complex in Step 1. In the presence of both UBC2 and UEV1 the ubiquitin is transferred onto UBC2 in Step 2 and then directed into diubiquitin species including K63-linked diubiquitin in Step 3. In the absence of UEV1, Ub from UBA1a-Ub is transferred to UBC2 in Step 4. In the presence of a cognate E3 ligase (here RING1, RING2 or RING4) the Ub is assembled either into unanchored Ub chains and/or used to autoubiquitylate E1/E2/E3 components present in the reaction mix (Step 5).

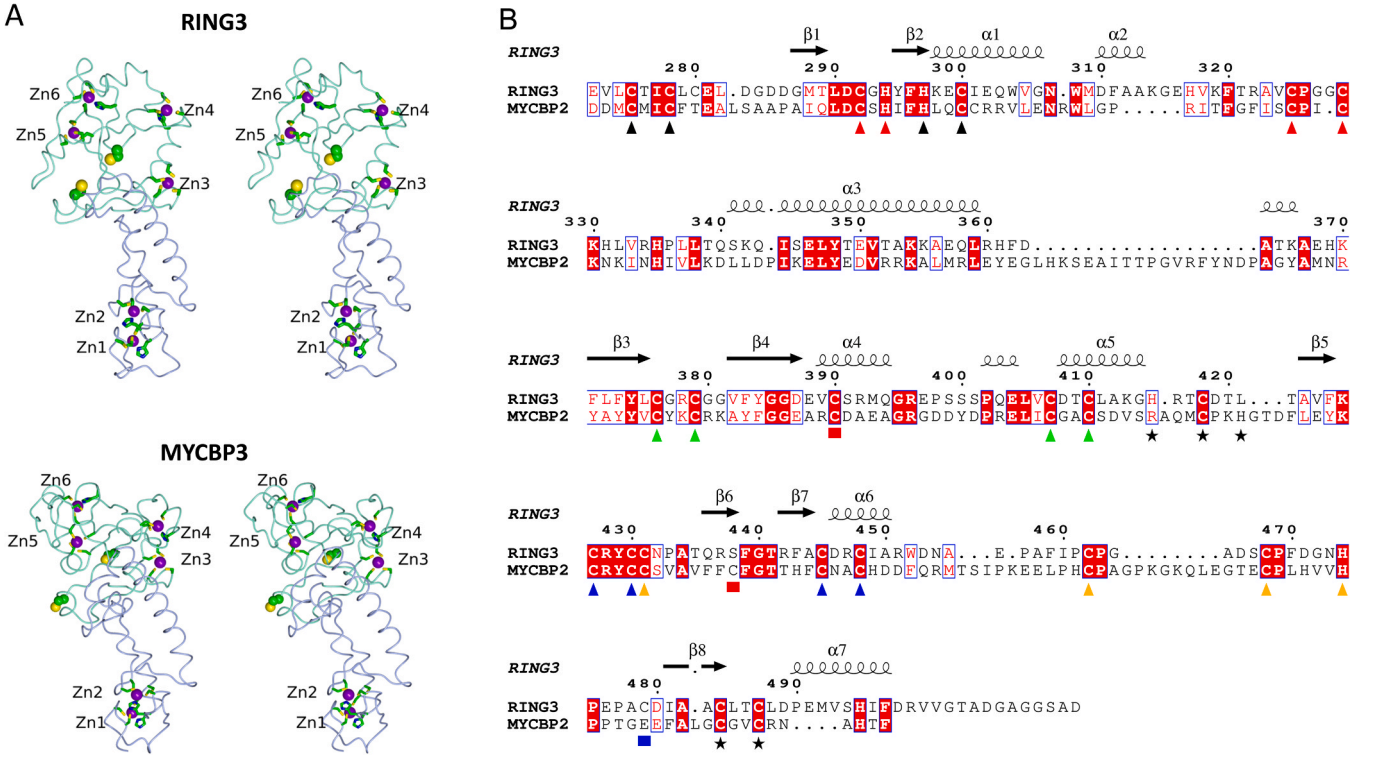

Fig. 4. Similarity of RING3 to human MYCBP2. A. Stereo worm representation of RING3 (upper) and MYCBP2 (lower). The chain is coloured by subdomains, the RING containing domain in ice blue and the TC domain in acquamarine. The zinc sites are numbered according to the order of the first coordinating residue in the polypeptide. Side chains of coordinating Cys and His resides are shown as cylinders. The Cys residues implicated in Ub transfer are shown as spheres. **B.** Sequence alignment of the zinc binding regions of RING3 (numbered) and MYCBP2. The secondary structure elements are from the AlphaFold model of RING3. The annotations below indicate the ligands of the various zincs – Zn1 black triangles: Zn2 red triangles; Zn3 green triangles; Zn4 black stars; Zn5 orange triangles; Zn6 purple triangles. For Zn4, the order of the first coordinating His and Cys ligand pair in RING3 is swapped in MYCBP2. The Cys residues implicated in Ub transfer in MYCBP2 are shown as red squares. A putative second acceptor in RING3 is marked with a blue square.

3. Discussion

UBC2 and UEV1 are ubiquitin E2 conjugating enzymes individually essential for promastigote to amastigote differentiation [13]. Parasites deficient in *UBC2* or *UEV1* die within 72 hrs of induction of differentiation [13]. To investigate the mechanism of this cell death and to explore further ubiquitination pathways in *Leishmania*, we identified the interaction partners of UBC2 and UEV1. Cross-linking affinity purification proteomics is a powerful and established method for identifying protein-protein interactions, defining protein networks and identifying substrates. The observation that UEV1 is significantly enriched in the UBC2 interactome and that UBC2 is enriched in the UEV1 interactome lends confidence to the quality of the data since UBC2 and UEV1 have been shown to form a stable heterodimeric functional complex *in vitro* [13]. Similarly, the prominence of ubiquitin system components in the UBC2 and UEV1 interactomes is consistent with the expected function of the two proteins. Ubiquitin was identified in the UBC2 interactome, which is consistent with the known mechanism of ubiquitination, where these two proteins form a covalent complex in the ubiquitination reaction cycle. The discovery of three RING E3 ligases in the UBC2 interactome suggests that these enzymes mediate transfer of ubiquitin from UBC2-Ub onto substrate proteins or onto other ubiquitin molecules. Assays with the purified RING1, RING2 and RING4 show that these factors can cooperate with UBC2 in the formation of ubiquitin conjugates. Given the defects of both Δ*ubc2* and Δ*uev1* null mutant parasites in amastigote formation, it will be important to determine whether the RING E3s identified here are required for differentiation to the human infectious forms.

Mechanistically, RING E3 ligases promote the transfer of ubiquitin from the donor E2-Ub complex to the receiver substrate without forming an E3-Ub covalent intermediate. They typically bind the E2-Ub in what is termed a closed complex which is reactive towards the side chain amines on lysine residues on acceptor substrates. RINGs 1, 2 and 4 clearly belong to this class which is distinct from the HECT and RBR-type E3 enzymes where an active site cysteine participates in a two-step transthiolation mechanism [22]. The analysis presented here suggests that RING 3 belongs to the newer and mechanistically distinct RING-Cys-Relay class of E3 ligases opening up the possibility of ubiquitin transfer to threonine residues on acceptor substrates. This warrants future investigation if the solubility problems associated with expression of this E3 can be overcome.

The discovery of a greater number of interacting partners for UBC2

than for UEV1 suggests that UBC2 has intracellular functions independent of UEV1, the most obvious being cooperation with the RING E3s in substrate ubiquitination. This is consistent with the capacity of UBC2 *in vitro* to cooperate with RING1, RING2 and RING4 to form ubiquitin chains in the absence of UEV1 [13]. The assay data presented here suggest that UEV1 prevents E3 mediated ubiquitin transfer, by diverting the ubiquitin from E2-Ub into K63-linked diubiquitin as observed previously [13]. The absence of the RING E3s in the UEV1 interactome, suggests that UBC2 binding to UEV1 and RING E3s are mutually exclusive *in vivo*.

The identification of UBC13 as an interacting partner for both UBC2 and UEV1 suggests that UBC2 and UBC13 may have distinct but complementary E2 activities, similar to those exhibited by human UBE2W and UBE2N-UBE2V1 [31–33]. UBC2 and UBC13 share 50% sequence identity. UBC13 is likely to be essential in promastigotes since null mutants were not obtained in the deletion mutagenesis study [13].

The remaining UBC2 interactors are potential UBC2 (or UBC2-UEV1) substrates. The interaction of UBC2 with aldose 1-epimerase-like protein, UDP-glucose 4'epimerase and isocitrate dehydrogenase points to roles for UBC2 in the regulation of carbohydrate metabolism [34,35]. Aldose 1-epimerase catalyses the interconversion of hexose sugars, such as glucose, between their α- and β- anomers, while UDP-glucose 4'epimerase reversibly converts UDP-galactose into UDP-glucose. Isocitrate dehydrogenase catalyses a key step in the citric acid cycle linking sugar utilisation and respiration. These findings are consistent with transcriptomics data showing changes in the levels of expression of genes associated with glycolysis and the citric acid cycle between amastigotes and promastigotes [36]. Ubiquitin modifications could contribute to regulation by altering the activity, localisation or degradation of target enzymes. UBC2 may also regulate gene expression, as implied by its interaction with the LSD1-like protein and endoribonuclease L-PSP (pb5). In humans, LSD1 is primarily responsible for the demethylation of mono- and dimethyl histone H3 lysine 4 (H3K4) and, interestingly, its aberrant activity has been linked with increased glycolytic activity in cancer cells [37]. Consequently, facilitating ubiquitination of the LSD1-like protein may be an additional way in which UBC2 regulates metabolism.

The identification of Rab-GDP dissociation inhibitor, kinesin, RAB11 GTPase and the small GTP-binding protein, whose functions are linked to intracellular transport, suggests that UBC2 may regulate trafficking and/or signalling. In *S. cerevisiae* and *C. elegans,* homologues of UBC2 have been shown to regulate membrane protein sorting [38,39]. The interaction of UBC2 with the vacuolar ATP synthase may also be significant in this regard. Components of the vacuolar ATP synthase were identified in a screen for *T. brucei* isometamidium resistance, suggesting a role for UBC2 in trypanosomal drug resistance [40]. Since K63 ubiquitin modifications provide signals for plasma membrane protein internalisation and other intracellular trafficking steps, the ubiquitination of the vacuolar ATPase by UBC2 could be proposed to influence its trafficking [41]. In *T. brucei*, the Gim5A protein is a glycosomal membrane protein essential for the survival of bloodstream-form trypanosomes (Maier et al., 2001). Its orthologue LmxM.34.3700 was found here to interact with UBC2 (Table 1). Whether UBC2 is involved in the trafficking of this Gim5A orthologue to the glycosomal membrane is an additional area for future investigation. The fact that UEV1 shares interactions with UBC13, Rab-GDP dissociation inhibitor and isocitrate dehydrogenase suggest that UEV1 cooperates with UBC2 in regulating cellular respiration and intracellular transport. Finally, the hypothetical protein, LmxM.26.2490 (1477 residues) is prominent in both the 3xMyc-UBC2 and 3xMyc-UEV1 samples; further study into the function of this protein is warranted. The same is true for two other hypothetical proteins, LmxM.30.2560 (1031 residues) and LmxM.28.0980 (240 residues), which are strongly enriched in the UBC2 and UEV1 interactomes respectively (Tables 1 and 2).

In conclusion, the studies presented here have defined a discrete set of interaction partner proteins for two ubiquitination factors required for development in *Leishmania* parasites. Future studies of the identified components promise to shed light on the differentiation process and its regulation.

4. Experimental procedures

4.1. Cell culture

L. mexicana (MNYC/BZ/62/M379) promastigotes were grown in HOMEM (Gibco) supplemented with 10% v/v heat-inactivated Fetal Bovine Serum (FBS) (Gibco) and 1% v/v Penicillin/Streptomycin (Sigma-Aldrich) at 25°C. Typically, cells were split around twice a week. Selection drugs were added to the medium as appropriate: 10 μg ml^{-1} blasticidin (InvivoGen), 40 μg ml^{-1} puromycin (InvivoGen), 50 μg ml^{-1} hygromycin (InvivoGen) and 50 μg ml^{-1} nourseothricin (Jena Bioscience).

4.2. Amastigote viability assay

L. mexicana promastigote cultures were grown to stationary phase and resuspended at 1 $\times 10^6$ cells per ml in amastigote medium (Schneider's Drosophila medium (Gibco), 20% FBS (Gibco) and 15 μg ml^{-1} Hemin (Sigma), adjusted to pH 5.5). 200 μl cell samples were incubated for 0 h, 48 h and 120 h prior to addition of 20 μl of 125 μg ml^{-1} resazurin (in 1 x PBS). Cells were then incubated at 37°C for 8 h and the fluorescence at 590 nm recorded using the POLARstar Omega Plate Reader (BMG Labtech). Data were normalized to the Cas9 T7 parental cell lines and presented as an average of two biological replicates, each with six technical replicates.

4.3. Generation of CRISPR-Cas9 edited lines

N-terminally myc-tagged lines were generated using a CRISPR-Cas9-based approach [5,21]. Primer sequences for amplification of the single guide DNAs (sgDNAs) and repair cassettes for tagging were designed using a web tool (http://www.leishgedit.net/Home.html). A summary of the primers used for generating myc-tagged lines and for diagnostic PCRs can be found in Supplementary Data 1.

PCR reactions for cassette amplification contained 30 ng of plasmid template DNA (pPLOTv1 blast-mNeonGreen-blast or pPLOTv1 puro-mNeonGreen-puro (20)), 0.2 mM dNTPs, 2 μM each of forward and reverse primer, 1 U Q5® DNA Polymerase (NEB), 1x Q5 reaction buffer (NEB) and distilled water to make the volume up to 40 μl. The PCR was run with the following settings: 94°C for 5 min, 45 cycles of 94°C for 30 s, 65°C for 30 sec and 72°C for 2 min 15 s and 72°C for 7 min. For the gRNAs, PCR reactions were set up in a similar manner but with a total volume of 20 μl. The PCR program used was 98°C for 30 s, 35 cycles of 98°C for 10 s, 60°C for 30 sec and 72°C for 15 s and 72°C for 10 min.

Transfection reactions contained around 1 $\times 10^6$ parasites and 5 μl of purified DNA from the PCRs; they were carried out using the P3 Primary Cell 4D-Nucleofector X Kit (Lonza) and the FI-115 program on the Amaxa 4D-Nucleofector (Lonza). Following recovery of the cells at 25°C, antibiotics were added to select for a population of transfectants.

4.4. Western blotting

Cells were resuspended in NuPAGE® LDS Sample Buffer [Thermo Scientific] supplemented with 7.5% β-mercaptoethanol and loaded onto a NuPAGE 4–12% Bis-Tris gel (ThermoFisher Scientific). Each lane contained protein derived from 1.3 $\times 10^6$ promastigotes and electrophoresis was carried out at 200 V for around 40 min. Following incubation of the gel in 20% ethanol for 10 min, blotting onto PVDF membranes was carried out with an iBlot™ 2 (Thermo Fisher Scientific) system, operated at 20 V for 1 min, 23 V for 4 min and 25 V for 7 min. The membrane was subsequently blocked in 5% milk in Tris-Buffered Saline with 0.05% Tween 20 (TBST, Sigma-Aldrich) for 1 h at room

temperature. Primary antibodies were incubated with the membrane for 1 h at room temperature or overnight at 4°C in 5% milk. After washing, secondary antibodies were incubated for 1 h at room temperature in 5% milk. For the anti-myc blot, anti-rabbit myc primary (polyclonal, abcam, ab9106) and StarBright™ Blue 700 Goat Anti-Rabbit IgG secondary (Bio-Rad) antibodies, both at 1:5000 dilution, were used. For the anti-OPB blot, anti-OPB primary antibody at 1:50,000 dilution, and Easy-Blot anti-sheep IgG (HRP) second antibody (GeneTex, GTX628906–01, Lot:41229) at 1:1000 dilution, were used. Membranes were washed, incubated with Clarity™ Max Western ECL Substrate (both Bio-Rad) and imaged using a ChemiDoc system (Bio-Rad).

4.5. Immunoprecipitation of myc-tagged proteins

Triplicate parasite samples were washed twice in PBS and resuspended in PBS containing 10 mM dithiobis(succinimidyl propionate) (Thermo Fisher Scientific) crosslinker. Crosslinking was allowed to proceed for 10 min at 25°C, and was quenched by addition of 20 mM Tris, pH 7.5. Parasites were harvested by centrifugation and resuspended in lysis buffer composed of 50 mM Tris, pH 7.5, 250 mM NaCl, 1 mM EDTA and the non-ionic detergent NP-40 (1%, Sigma-Aldrich) which was supplemented with protease inhibitors: 3.3 x cOmplete™, Mini, EDTA-free Protease Inhibitor Cocktail (Roche), 1 x PhosSTOP™ (Roche), 1.5 mM Pepstatin A (Sigma-Aldrich), 1 mM PMSF (Sigma-Aldrich), 10 μM E64, 0.4 μM 1–10 phenanthroline (Sigma-Aldrich) and 2 x Proteoloc™ Protease Inhibitor Cocktail (Expedeon) on ice. For each sample, 8 $\times 10^8$ cells were lysed in 400 μl lysis buffer. The suspension was next sonicated on ice with three 10 sec pulses at amplitude 25, at 60 second intervals. The lysates were clarified by centrifugation at 10,000 x g for 10 min at 4°C. To enrich for myc-tagged proteins, 30 μl of Pierce™ Anti-c-Myc Magnetic Beads (Thermo Fisher Scientific) were added to each sample. Affinity purification was carried out for 2.5 h at 4°C with end-over-end rotation. Following incubation, beads were washed four times in 300 μl lysis buffer, leaving on ice for 5 min between each wash. Beads were then resuspended in 300 μl PBS and washed twice in 300 μl PBS. Myc-tagged proteins were eluted from the beads by adding 0.1 M glycine, pH 2 and vortexing at 700 rpm for 15 min at room temperature. 1 M Tris-HCl, pH 8.5 at one tenth of the sample volume was added to neutralise the acid and the elution step repeated twice.

4.6. Mass spectrometry sample preparation

Following elution from the beads, 4 volumes of methanol and 1 vol of chloroform were added to the samples, which were subsequently vortexed for 0.5–1 min. This was followed by centrifugation at 17,000 x g for 1 h at 4°C. The pellet was then washed with 3 volumes of methanol, resuspended in 150 μl 50 mM triethylammonium bicarbonate (TEAB), pH 8.5 containing 0.1% PPS silent surfactant (Expedeon) and incubated for 1 h at room temperature with shaking. To reduce and alkylate proteins, 10 mM tris(2-carboxyethyl)phosphine (TCEP) and 10 mM iodoacetamide (VWR Life Science) were added and the mixture was incubated for 30 min at room temperature in the dark. To digest the proteins, 200 ng of Trypsin/Lys-C Mix (Promega) and 1 mM $CaCl_2$ was added, and the samples were incubated at 37°C overnight with shaking. Following centrifugation, the supernatant was retained and acidified by addition of trifluoroacetic acid (TFA) to a final concentration of 0.5% before centrifugation for 10 mins at 17,000 x g. Peptides were desalted using C18 desalting tips prepared in-house and eluted in 60 μl of 80% acetonitrile, 0.1% TFA. Desalted peptides were dried and stored at −20°C prior to mass spectrometry analysis.

4.7. Mass spectrometry data acquisition

Samples were loaded onto an mClass UPLC system (Waters) equipped with a nanoEase M/Z Symmetry C_{18} Trap Column (100 Å, 5 μm, 180 μm x 20 mm, Waters) and a PepMap, C_{18} EasyNano nanocapillary column (100 Å, 2 μm, 75 μm x 150 mm, Thermo). The trap wash solvent was aqueous 0.1% (v:v) trifluoroacetic acid and the trapping flow rate was 15 μl/min. The trap was washed for 5 min before switching flow to the capillary column. Separation used gradient elution of two solvents: solvent A, aqueous 1% (v:v) formic acid; solvent B, acetonitrile containing 1% (v:v) formic acid. The flow rate for the capillary column was 300 nl/min and the column temperature was 40°C. The linear multi-step gradient profile was: 3–10% B over 7 mins, 10–35% B over 30 mins, 35–99% B over 5 mins and then proceeded to wash with 99% solvent B for 4 min. The column was returned to its initial conditions and re-equilibrated for 15 min before subsequent injections.

The nanoLC system was interfaced with an Orbitrap Fusion Tribrid mass spectrometer (Thermo) with an EasyNano ionisation source (Thermo). Positive ESI-MS and MS^2 spectra were acquired using Xcalibur software (version 4.0, Thermo). Instrument source settings were: ion spray voltage, 1900 V; sweep gas, 0 Arb; ion transfer tube temperature; 275°C. MS^1 spectra were acquired in the Orbitrap with: 120,000 resolution, scan range: *m/z* 375–1500; AGC target, $4e^5$; max fill time, 100 ms. Data dependent acquisition was performed in top speed mode using a 1 s cycle, selecting the most intense precursors with charge states >1. Easy-IC was used for internal calibration. Dynamic exclusion was performed for 50 s post precursor selection and a minimum threshold for fragmentation was set at $5e^3$. MS^2 spectra were acquired in the linear ion trap with: scan rate, turbo; quadrupole isolation, 1.6 *m/z*; activation type, HCD; activation energy: 32%; AGC target, $5e^3$; first mass, 110 *m/z*; max fill time, 100 ms. Acquisitions were arranged by Xcalibur to inject ions for all available parallelizable time.

4.8. Mass spectrometry data analysis

Peak lists in.raw format were imported into Progenesis QI (Version 2.2., Waters) for peak picking and chromatographic alignment. Precursor ion intensities were normalised against total intensity for each acquisition. A combined peak list was exported in.mgf format for database searching against the *L. mexicana* subset of the TriTrypDB database (8250 sequences; 5180,224 residues), appended with common proteomic contaminants. (116 sequences; 38,371 residues). Mascot Daemon (version 2.6.0, Matrix Science) was used to submit the search to a locally-running copy of the Mascot program (Matrix Science Ltd., version 2.7.0). Search criteria specified: Enzyme, trypsin; Max missed cleavages, 2; Fixed modifications, Carbamidomethyl (C); Variable modifications, Oxidation (M), Phosphorylation (S,T,Y), Ubiquitin (K); Peptide tolerance, 3 ppm; MS/MS tolerance, 0.5 Da; Instrument, ESI-TRAP. Peptide identifications were passed through the percolator algorithm to achieve a 1% false discovery rate assessed against a reverse database and individual matches filtered to require minimum expect score of 0.05. The Mascot.XML result file was imported into Progenesis QI and peptide identifications associated with precursor peak areas were then matched between runs. Relative protein abundance was calculated using precursor ion areas from non-conflicting unique peptides. Accepted protein quantifications were set to require a minimum of two unique peptide sequences.

In this analysis, proteins were reported based on the rule of parsimony, meaning that where two or more proteins shared identical peptides, the shortest protein alone was presented as the simplest way to explain the data. Proteins with >1 missing value in each sample group of 3 replicates were removed. For remaining proteins, putative UBC2 and UEV1 interactors were scored using SAINTq (23) with missing value imputation enabled, comparing against the control (MPK3) immunoprecipitation. A false discovery rate threshold of < 5% was applied to select for high confidence interactors. The identification of key processes associated with UBC2 and UEV1 interacting partners was facilitated by gene ontology (GO) enrichment in TriTrypDB and literature searching.

4.9. Cloning and expression

Codon-optimised sequences encoding RING1, RING2 and RING4 were cloned into a modified pET-YSBLIC [42] plasmid downstream of sequences encoding glutathione S transferase (GST) and a cleavage recognition sequence for human rhinovirus 3 C (HRV-3 C) protease. The resulting GST-3C-RING fusion protein coding sequences were transcribed from a T7 promoter under the control of a *lac* operator. GST-3C-RING1 was produced in *E. coli* LEMO21 (DE3) (NEB) grown in LB media supplemented with 30 μg ml^{-1} kanamycin and 50 μg ml^{-1} chloramphenicol. Cells were grown at 37°C with shaking at 180 rpm to an OD_{600} of 0.7 before induction with 0.4 mM IPTG and growth overnight at 18°C with shaking at 180 rpm. GST-3C-RING2 was expressed in BL21 gold grown in LB supplemented with 30 μg ml^{-1} kanamycin. Cells were induced with 1 mM IPTG but otherwise cultured as described for RING1. GST-3C-RING4 was expressed in BL21 (DE3) grown in LB and supplemented with 30 μM ml^{-1} kanamycin and 250 μM zinc chloride.

4.10. Protein purification

Ubiquitin (Cat No U-100 H-10 M), was obtained from R&D Systems. The monoclonal antibody FK2 was from Ubiquigent (68–0121–500) and the mouse anti-human Ub-K63 antibody was from Affymetrix eBioscience (14–6077–82). Protocols for the construction of vectors for the expression in *E. coli* of sequences encoding UBA1a, UBC2 and UEV1 from *L. mexicana* have been described together with protocols for the purification of the recombinant proteins (13). For the purification of the RING E3 ligases, cell pellets were resuspended in a lysis buffer of 50 mM Hepes pH 7.5, 300 mM NaCl supplemented with a Complete protease inhibitor tablet (Roche) and lysed by sonication. The soluble cell lysate was applied to a 5 ml GSTrap FF column and an on-column cleavage of the GST-tag was performed by incubation with 50 μg ml^{-1} 3 C protease overnight. Cleaved RING protein was washed off the column with 5 column volumes of 50 mM Hepes pH 7.5, 300 mM NaCl. The protein was subsequently concentrated using a 10 kDa cut-off concentrator (Amicon) and further purified by size-exclusion chromatography using an S75 16/600 column run at 1 ml min^{-1} in a buffer of 50 mM Hepes pH 7.5, 300 mM NaCl.

4.11. E3 cooperation assay

A detailed assay protocol for assessing E3 cooperation has been described (25). In the control experiments shown in Supplementary Figure 5, reaction mixes contained 300 nM UBA1a, and 100 μM ubiquitin in a buffer of 50 mM HEPES pH 7.5, 100 mM NaCl, 10 mM $MgCl_2$, 2 mM DTT, in the presence and absence of either 3.1 μM UBC2 and or/ 10 mM ATP in a total volume of 20 μL. These reactions were run for 30 mins at 30°C following which non-reducing sample buffer was added and the samples resolved by SDS-PAGE and visualisation with Instant Blue stain. For the RING E3 ligase assays, reaction mixes were prepared containing 100 nM UBA1a, 2.5 μM UBC2, 2.5 μM UEV1, 1.0 μM RING E3 ligase and 100 μM ubiquitin in a buffer of 50 mM HEPES pH 7.5, 100 mM NaCl, 10 mM $MgCl_2$, 2 mM DTT, 5 mM ATP in a total volume of 40 μL. Four control reactions were carried out in which either the RING E3 ligase, UBC2, UEV1 or both UBC2 and UEV1 were omitted. Reactions were incubated at 37°C for 1 hour before quenching by the addition of 1x SDS-sample buffer. The formation of ubiquitin conjugates was assessed by western blotting using FK2-antibody (Ubiquigent) or, for assessment of K63-linkages, Ub-K63 antibody (Thermofisher) as the primary antibody and an HRP-conjugated mouse secondary antibody for detection.

Funding and Additional Information

This work was supported by a Medical Research Council award of a Studentship to RB (MRC MR/N018230/), Grant MR/K019384/1 to JCM and a Wellcome Trust award to JCM (200807/Z/16/Z).

Declaration of Competing Interest

The authors Rebecca J. Burge, Katie H. Jameson, Vincent Geoghegan, Adam Dowle, Jeremy C. Mottram and Anthony J. Wilkinson of the manuscript 'Formation of functional E3 ligase complexes with UBC2 and UEV1 of *Leishmania mexicana*' being submitted for publication in *Molecular and Biochemical Parasitology* have no interests to declare.

Acknowledgements

We thank Sergios Antoniou, Jim Brannigan and Nathaniel Jones for helpful discussions, We are grateful to the York Centre of Excellence in Mass Spectrometry which was created thanks to a major capital investment through Science City York, supported by Yorkshire Forward with funds from the Northern Way Initiative, and subsequent support from EPSRC (EP/K039660/1; EP/M028127/1).

Author Contributions

The project was conceived by RJB and JCM with input from AJW. The parasite and proteomics work was carried out by RJB with mass spectrometry data collection by AAD and analysis by VG. Protein purification and enzyme assays were performed by KHJ. The manuscript was drafted by RJB and AJW, and edited and revised by all authors.

Appendix A. Supporting information

Supplementary data associated with this article can be found in the online version at doi:10.1016/j.molbiopara.2024.111619.

References

[1] S. Burza, S.L. Croft, M. Boelaert, Leishmaniasis, Lancet 392 (2018) 951–970.
[2] S. Sasidharan, P. Saudagar, Leishmaniasis: where are we and where are we heading? Parasitol. Res. 120 (2021) 1541–1554.
[3] S. Mann, K. Frasca, S. Scherrer, A.F. Henao-Martinez, S. Newman, P. Ramanan, J. A. Suarez, A review of Leishmaniasis: current knowledge and future directions, Curr. Trop. Med. Rep. 8 (2021) 121–132.
[4] A. Nagle, A. Biggart, C. Be, H. Srinivas, A. Hein, D. Caridha, R.J. Sciotti, B. Pybus, M. Kreishman-Deitrick, B. Bursulaya, Y.H. Lai, M.Y. Gao, F. Liang, C.J.N. Mathison, X. Liu, V. Yeh, J. Smith, I. Lerario, Y. Xie, D. Chianelli, M. Gibney, A. Berman, Y. L. Chen, J. Jiricek, L.C. Davis, X. Liu, J. Ballard, S. Khare, F.K. Eggimann, A. Luneau, T. Groessl, M. Shapiro, W. Richmond, K. Johnson, P.J. Rudewicz, S.P. S. Rao, C. Thompson, T. Tuntland, G. Spraggon, R.J. Glynne, F. Supek, C. Wiesmann, V. Molteni, Discovery and characterization of clinical candidate LXE408 as a kinetoplastid-selective proteasome inhibitor for the treatment of Leishmaniases, J. Med. Chem. 63 (2020) 10773–10781.
[5] N. Baker, C.M.C. Catta-Preta, R. Neish, J. Sadlova, B. Powell, E.V.C. Alves-Ferreira, V. Geoghegan, J.B.T. Carnielli, K. Newling, C. Hughes, B. Vojtkova, J. Anand, A. Mihut, P.B. Walrad, L.G. Wilson, J.W. Pitchford, P. Volf, J.C. Mottram, Systematic functional analysis of Leishmania protein kinases identifies regulators of differentiation or survival, Nat. Commun. 12 (2021) 1244.
[6] R.J. Burge, J.C. Mottram, A.J. Wilkinson, Ubiquitin and ubiquitin-like conjugation systems in trypanosomatids, Curr. Opin. Microbiol. 70 (2022) 102202.
[7] A. Zuin, M. Isasa, B. Crosas, Ubiquitin signaling: extreme conservation as a source of diversity, Cells 3 (2014) 690–701.
[8] N. Zheng, N. Shabek, Ubiquitin Ligases: structure, function, and regulation, Annu Rev. Biochem 86 (2017) 129–157.
[9] D. Komander, M. Rape, The ubiquitin code, Annu Rev. Biochem. 81 (2012) 203–229.
[10] T.E.T. Mevissen, D. Komander, Mechanisms of deubiquitinase specificity and regulation, Annu Rev. Biochem 86 (2017) 159–192.
[11] M. Karpiyevich, K. Artavanis-Tsakonas, Ubiquitin-like modifiers: emerging regulators of protozoan parasites, Biomolecules 10 (2020).
[12] M.J. Bijlmakers, Ubiquitination and the proteasome as drug targets in trypanosomatid diseases, Front Chem. 8 (2021).
[13] R.J. Burge, A. Damianou, A.J. Wilkinson, B. Rodenko, J.C. Mottram, Leishmania differentiation requires ubiquitin conjugation mediated by a UBC2-UEV1 E2 complex, PLoS Pathog. 16 (2020) e1008784.
[14] A. Damianou, R.J. Burge, C.M.C. Catta-Preta, V. Geoghegan, Y.R. Nievas, K. Newling, E. Brown, R. Burchmore, B. Rodenko, J.C. Mottram, Essential roles for deubiquitination in Leishmania life cycle progression, PLoS Pathog. 16 (2020) e1008455.

[15] J.S. Grewal, C.M.C. Catta-Preta, E. Brown, J. Anand, J.C. Mottram, Evaluation of clan CD C11 peptidase PNT1 and other Leishmania mexicana cysteine peptidases as potential drug targets, Biochimie 166 (2019) 150–160.
[16] S. Alsford, D.J. Turner, S.O. Obado, A. Sanchez-Flores, L. Glover, M. Berriman, C. Hertz-Fowler, D. Horn, High-throughput phenotyping using parallel sequencing of RNA interference targets in the African trypanosome, Genome Res 21 (2011) 915–924.
[17] T.F. Moraes, R.A. Edwards, S. McKenna, L. Pastushok, W. Xiao, J.N. Glover, M. J. Ellison, Crystal structure of the human ubiquitin conjugating enzyme complex, hMms2-hUbc13, Nat. Struct. Biol. 8 (2001) 669–673.
[18] M.J. Eddins, C.M. Carlile, K.M. Gomez, C.M. Pickart, C. Wolberger, Mms2-Ubc13 covalently bound to ubiquitin reveals the structural basis of linkage-specific polyubiquitin chain formation, Nat. Struct. Mol. Biol. 13 (2006) 915–920.
[19] A.P. VanDemark, R.M. Hofmann, C. Tsui, C.M. Pickart, C. Wolberger, Molecular insights into polyubiquitin chain assembly: crystal structure of the Mms2/Ubc13 heterodimer, Cell 105 (2001) 711–720.
[20] T. Beneke, E. Gluenz, LeishGEdit: a method for rapid gene knockout and tagging using CRISPR-Cas9, Methods Mol. Biol. 1971 (2019) 189–210.
[21] T. Beneke, R. Madden, L. Makin, J. Valli, J. Sunter, E. Gluenz, A CRISPR Cas9 high-throughput genome editing toolkit for kinetoplastids, R. Soc. Open Sci. 4 (2017) 170095.
[22] M.B. Metzger, J.N. Pruneda, R.E. Klevit, A.M. Weissman, RING-type E3 ligases: master manipulators of E2 ubiquitin-conjugating enzymes and ubiquitination, Biochim Biophys. Acta 1843 (2014) 47–60.
[23] G. Teo, H. Koh, D. Fermin, J.P. Lambert, J.D. Knight, A.C. Gingras, H. Choi, SAINTq: Scoring protein-protein interactions in affinity purification - mass spectrometry experiments with fragment or peptide intensity data, Proteomics 16 (2016) 2238–2245.
[24] J. Jumper, R. Evans, A. Pritzel, T. Green, M. Figurnov, O. Ronneberger, K. Tunyasuvunakool, R. Bates, A. Zidek, A. Potapenko, A. Bridgland, C. Meyer, S.A. A. Kohl, A.J. Ballard, A. Cowie, B. Romera-Paredes, S. Nikolov, R. Jain, J. Adler, T. Back, S. Petersen, D. Reiman, E. Clancy, M. Zielinski, M. Steinegger, M. Pacholska, T. Berghammer, S. Bodenstein, D. Silver, O. Vinyals, A.W. Senior, K. Kavukcuoglu, P. Kohli, D. Hassabis, Highly accurate protein structure prediction with AlphaFold, Nature 596 (2021) 583–589.
[25] R.J. Burge, K.H. Jameson, A.J. Wilkinson, J.C. Mottram, In vitro Di-ubiquitin formation assay and E3 cooperation assay, Bio Protoc. 12 (2022).
[26] P.Y. Wu, M. Hanlon, M. Eddins, C. Tsui, R.S. Rogers, J.P. Jensen, M.J. Matunis, A. M. Weissman, C. Wolberger, C.M. Pickart, A conserved catalytic residue in the ubiquitin-conjugating enzyme family, EMBO J. 22 (2003) 5241–5250.
[27] Q. Yin, S.C. Lin, B. Lamothe, M. Lu, Y.C. Lo, G. Hura, L.X. Zheng, R.L. Rich, A. D. Campos, D.G. Myszka, M.J. Lenardo, B.G. Darnay, H. Wu, E2 interaction and dimerization in the crystal structure of TRAF6, Nat. Struct. Mol. Biol. 16 (2009), 658-U697.
[28] M.J. Bijlmakers, J.M.C. Teixeira, R. Boer, M. Mayzel, P. Puig-Sàrries, G. Karlsson, M. Coll, M. Pons, B. Crosas, A C2HC zinc finger is essential for the RING-E2 interaction of the ubiquitin ligase RNF125, Sci. Rep. -Uk 6 (2016).
[29] P.D. Mabbitt, A. Loreto, M.A. Dery, A.J. Fletcher, M. Stanley, K.C. Pao, N.T. Wood, M.P. Coleman, S. Virdee, Structural basis for RING-Cys-Relay E3 ligase activity and its role in axon integrity, Nat. Chem. Biol. 16 (2020) 1227–1236.
[30] K.C. Pao, N.T. Wood, A. Knebel, K. Rafie, M. Stanley, P.D. Mabbitt, R. Sundaramoorthy, K. Hofmann, D.M.F. van Aalten, S. Virdee, Activity-based E3 ligase profiling uncovers an E3 ligase with esterification activity, Nature 556 (2018) 381–385.
[31] S.E. Soss, Y. Yue, S. Dhe-Paganon, W.J. Chazin, E2 conjugating enzyme selectivity and requirements for function of the E3 ubiquitin ligase CHIP, J. Biol. Chem. 286 (2011) 21277–21286.
[32] Y. Ye, M. Rape, Building ubiquitin chains: E2 enzymes at work, Nat. Rev. Mol. Cell Biol. 10 (2009) 755–764.
[33] M. Zhang, M. Windheim, S.M. Roe, M. Peggie, P. Cohen, C. Prodromou, L.H. Pearl, Chaperoned ubiquitylation–crystal structures of the CHIP U box E3 ubiquitin ligase and a CHIP-Ubc13-Uev1a complex, Mol. Cell 20 (2005) 525–538.
[34] B. Poolman, T.J. Royer, S.E. Mainzer, B.F. Schmidt, Carbohydrate utilization in Streptococcus thermophilus: characterization of the genes for aldose 1-epimerase (mutarotase) and UDPglucose 4-epimerase, J. Bacteriol. 172 (1990) 4037–4047.
[35] P.A. Frey, The Leloir pathway: a mechanistic imperative for three enzymes to change the stereochemical configuration of a single carbon in galactose, FASEB J. 10 (1996) 461–470.
[36] M. Fiebig, S. Kelly, E. Gluenz, Comparative life cycle transcriptomics Revises Leishmania mexicana genome annotation and links a chromosome duplication with parasitism of vertebrates, PLoS Pathog. 11 (2015) e1005186.
[37] A. Sakamoto, S. Hino, K. Nagaoka, K. Anan, R. Takase, H. Matsumori, H. Ojima, Y. Kanai, K. Arita, M. Nakao, Lysine demethylase LSD1 coordinates glycolytic and mitochondrial metabolism in hepatocellular carcinoma cells, Cancer Res 75 (2015) 1445–1456.
[38] C. Renz, V. Albanese, V. Troster, T.K. Albert, O. Santt, S.C. Jacobs, A. Khmelinskii, S. Leon, H.D. Ulrich, Ubc13-Mms2 cooperates with a family of RING E3 proteins in budding yeast membrane protein sorting, J. Cell Sci. 133 (2020).
[39] J. Zhang, J. Liu, A. Norris, B.D. Grant, X. Wang, A novel requirement for ubiquitin-conjugating enzyme UBC-13 in retrograde recycling of MIG-14/Wntless and Wnt signaling, Mol. Biol. Cell 29 (2018) 2098–2112.
[40] N. Baker, G. Hamilton, J.M. Wilkes, S. Hutchinson, M.P. Barrett, D. Horn, Vacuolar ATPase depletion affects mitochondrial ATPase function, kinetoplast dependency, and drug sensitivity in trypanosomes, Proc. Natl. Acad. Sci. USA 112 (2015) 9112–9117.
[41] Z. Erpapazoglou, O. Walker, R. Haguenauer-Tsapis, Versatile roles of k63-linked ubiquitin chains in trafficking, Cells 3 (2014) 1027–1088.
[42] M.J. Fogg, A.J. Wilkinson, Higher-throughput approaches to crystallization and crystal structure determination, Biochem Soc. Trans. 36 (2008) 771–775.
[43] P. Emsley, B. Lohkamp, W.G. Scott, K. Cowtan, Features and development of Coot, Acta Crystallogr D. Biol. Crystallogr 66 (2010) 486–501.
[44] S. McNicholas, E. Potterton, K.S. Wilson, M.E. Noble, Presenting your structures: the CCP4mg molecular-graphics software, Acta Crystallogr D. Biol. Crystallogr 67 (2011) 386–394.